Iranian Journal of Basic Medical Sciences
ijbms.mums.ac.ir

Syringic acid attenuates LPS-induced acute lung injury via modulation of the HMGB1/TLR4/NF-κB and Keap1/Nrf2/HO-1 pathways: Mechanistic insights from *in vivo* and *in silico* studies

Burak Batuhan Lacin [1], Emin Sengul [1, 2], Serkan Yildirim [3, 4], Furkan Aykurt [1], Mohamad Warda [1, 5], Burak Cinar [2], Ali Cinar [1]*

[1] Department of Physiology, Faculty of Veterinary Medicine, Ataturk University, Erzurum, Turkey
[2] Department of Pharmacology, Faculty of Medicine, Atatürk University, Erzurum, Turkey
[3] Department of Pathology, Faculty of Veterinary Medicine, Ataturk University, Erzurum, Turkey
[4] Department of Pathology, Faculty of Veterinary Medicine, Kyrgyzstan-Turkey Manas University, Bishkek, Kyrgyzstan
[5] Department of Biochemistry, Faculty of Veterinary Medicine, Cairo University, Giza, Egypt

ARTICLE INFO

Article type:
Original

Article history:
Received: Aug 1, 2025
Accepted: Oct 27, 2025

Keywords:
Acute lung Injury
Inflammation
Lipopolysaccharide
NF-kappa B
Oxidative stress
Phenols

ABSTRACT

Objective(s): Sepsis-induced acute lung injury (ALI), driven by uncontrolled inflammation and oxidative stress, remains a major cause of mortality in critically ill patients. This study aimed to investigate the protective and mechanistic effects of syringic acid (SA), a natural phenolic compound, against lipopolysaccharide (LPS)-induced ALI in rats.

Materials and Methods: Male Sprague–Dawley rats were allocated into five groups: control, SA80, LPS, SA40+LPS, and SA80+LPS. SA was orally administered (40 or 80 mg/kg/day) for 14 days before a single intraperitoneal injection of LPS (10 mg/kg). Lung tissues were collected 12 hr post-LPS for histopathological, biochemical, and molecular evaluations. In silico docking using Schrödinger Maestro (2025/1) assessed SA interaction with the KEAP1 Kelch domain (PDB: 5FZN).

Results: LPS challenge caused severe pulmonary edema, inflammatory infiltration, elevated proinflammatory cytokines, lipid peroxidation, and reduced antioxidant enzyme activities. SA pretreatment, particularly at 80 mg/kg, significantly ($P<0.05$) alleviated these alterations. Mechanistically, SA down-regulated the HMGB1/TLR4/NF-κB signaling cascade and activated the Keap1/Nrf2/HO-1 antioxidant pathway. Reduced 8-OHdG and caspase-3 expression indicated mitigation of oxidative DNA damage and apoptosis. Docking analysis revealed strong binding affinity and favorable MM-GBSA scores for SA within the KEAP1 active pocket, suggesting direct modulation of Nrf2 activation.

Conclusion: SA confers potent protection against LPS-induced ALI through coordinated anti-inflammatory and antioxidant mechanisms involving HMGB1/TLR4/NF-κB inhibition and Keap1/Nrf2/HO-1 activation. These findings highlight SA as a promising therapeutic candidate for sepsis-associated pulmonary injury.

▶Please cite this article as:
Lacin BB, Sengul E, Yildirim S, Aykurt F, Warda M, Cinar B, Cinar A. Syringic acid attenuates LPS-induced acute lung injury via modulation of the HMGB1/TLR4/NF-κB and Keap1/Nrf2/HO-1 pathways: Mechanistic insights from *in vivo* and *in silico* studies. Iran J Basic Med Sci 2026; 29: 302-312. doi: https://dx.doi.org/10.22038/ijbms.2026.90093.19427

Introduction

Sepsis remains a critical global health issue characterized by a dysregulated host response to infection that can lead to life-threatening organ dysfunction and high mortality rates (1). Among the organs affected, the lungs are notably vulnerable, making sepsis-induced lung injury a common and severe complication. This condition is characterized by acute inflammation and increased pulmonary microvascular permeability; however, despite extensive research, the underlying molecular mechanisms remain incompletely understood (2, 3).

Lipopolysaccharide (LPS), a major component of the outer membrane of Gram-negative bacteria, is widely used to model sepsis in experimental settings because it can trigger inflammatory responses (4-6). LPS-induced lung injury recapitulates many hallmarks of clinical sepsis-associated acute lung injury (ALI) and acute respiratory distress syndrome (ARDS), including massive neutrophil infiltration, oxidative stress, and an overwhelming release of proinflammatory cytokines such as TNF-α, IL-1β, and IL-6 (7, 8). Key pathways implicated in LPS-induced ALI include the pro-inflammatory TLR4/NF-κB signaling axis and the anti-oxidant Keap1/Nrf2/HO-1 pathway. Dysregulation of these pathways contributes to both excessive inflammation and oxidative injury in the lungs (9-11). High mobility group box 1 (HMGB1), a nuclear protein released in response to stress, acts as a damage-associated molecular pattern (DAMP) and amplifies inflammation by interacting with receptors such as TLR2, TLR4, and TLR9 (12-15).

Oxidative stress is a major contributor to LPS-induced

***Corresponding author:** Ali Cinar. Department of Physiology, Faculty of Veterinary Medicine, Ataturk University, Erzurum, Turkey. Email: bblacin@atauni.edu.tr

lung injury, arising from an imbalance between reactive oxygen species (ROS) production and anti-oxidant defenses such as superoxide dismutase (SOD) and glutathione peroxidase (GPx)(16). The Keap1/Nrf2/HO-1 signaling axis plays a central role in protecting against oxidative damage, regulating cytoprotective responses, and mitigating inflammation (17-21).

Syringic acid (SA), a naturally occurring phenolic compound (4-hydroxy-3,5-dimethoxybenzoic acid) found in various fruits and edible plants, has demonstrated anti-oxidant and anti-inflammatory effects (22-24). By scavenging ROS and modulating pathways such as Nrf2/Keap1/HO-1 and TLR4/HMGB1/NF-κB, SA may protect against oxidative stress and inflammation in LPS-induced ALI (23, 25). Despite its broad biological activities, including antimicrobial, antidiabetic, and anticancer effects (25, 26), the potential of SA in the treatment of sepsis-induced lung injury has not yet been evaluated.

To our knowledge, this is the first study to comprehensively evaluate the protective effects of SA against LPS-induced lung injury in rats, integrating biochemical, molecular, histopathological, immunofluorescence, and *in silico* approaches. This study aimed to explore whether SA can mitigate lung injury by modulating key pro-inflammatory and anti-oxidant pathways, providing insights into its therapeutic potential in septic lung injury.

Materials and Methods

Chemicals

Syringic acid (SA; CAS No: 530-57-4) was purchased from Bostonchem (Boston, MA, USA). Lipopolysaccharide (LPS; CAS No: 297-473-0, serotype O55:B5) and all other analytical-grade chemicals were obtained from Sigma-Aldrich (St. Louis, MO, USA). The enzyme-linked immunosorbent assay (ELISA) kits used in the study were supplied by SunRedBio (Shanghai, China).

Animals

Sixty adult male Sprague-Dawley rats (12 weeks old, 270-275 g) were obtained from the Medical Experimental Application and Research Center of Atatürk University. Before the experiment, all the animals were weighed and randomly assigned to five experimental groups. The rats were housed under controlled conditions: 25±2 ˚C, 60±10% relative humidity, and a 12-hour light/dark cycle. The animals had *ad libitum* access to standard food and water. A one-week acclimatization period was allowed before the experimental procedures began. The Local Ethics Committee approved all experimental protocols for Animal Experiments of Atatürk University (Approval No: 2022/181).

Experimental design

The doses of SA and LPS administered in this study were based on previously published protocols. The SA dosing regimen was adapted from Gheena *et al.* (2022)(27), and the LPS dose was selected according to Köse *et al.* (2021)(28). SA was administered intragastrically (i.g.) at 40 mg/kg and 80 mg/kg, whereas LPS was administered IP at 10 mg/kg.

The experimental groups were as follows:

Group I (control): 1 mL of saline was given i.g. for 14 days.

Group II (SA80): 80 mg/kg SA i.g. for 14 days.

In Group III (LPS), 1 mL of saline was given i.g. for 14 days, followed by a single dose of LPS (10 mg/kg, IP) 1 hr after the final saline administration.

Group IV (SA40+LPS): 40 mg/kg SA i.g. for 14 days, followed by a single dose of LPS (10 mg/kg, IP) 1 hr after the final SA administration.

Group V (SA80+LPS): 80 mg/kg SA i.g. for 14 days, followed by a single dose of LPS (10 mg/kg, IP) 1 hr after the final SA administration.

The rats were euthanized under sevoflurane anesthesia 12 hr after the final LPS administration on the 14th day.

Lung and body weights of the rats

The body weights of all the rats were recorded immediately before the experiment and again just before euthanasia. After euthanasia, the lungs were excised and weighed. The data were subsequently analyzed and compared across the experimental groups.

Homogenization of lung tissues

Lung tissues stored at -80 ˚C were placed in MagNA lyser tubes, and 1.5 mL of pH 7.4 PBS and a steel ball were added. The samples placed in the MagNA lyser device were subsequently homogenized at 6000 rpm for 60 sec. The recovered supernatants were then used to determine the following biochemical parameters in the rats' lungs, according to the procedures of the commercial ELISA kits, using an ELISA plate reader (Bio-Tek, Winooski, VT, USA).

Analyses of oxidative stress parameters in lung tissue

The oxidative stress markers malondialdehyde (MDA) (Cat. No: 201-11-0157), superoxide dismutase (SOD) (Cat. No: 201-11-0169), and glutathione peroxidase (GPx) (Cat. No: 201-11-5104) in lung tissue supernatants were quantified using commercial ELISA kits according to the manufacturer's instructions. The plate absorbance was measured using a BioTek ELISA reader (EPOCH II program) at 450 nm.

Analyses of inflammation parameters in lung tissue

Inflammatory cytokines, including tumor necrosis factor-alpha (TNF-α)(Cat. No: 201-11-0765), interleukin-1 beta (IL-1β)(Cat. No: 201-11-0120), and interleukin-6 (IL-6)(Cat. No: 201-11-0136), in the lung tissue supernatants were quantified via commercial ELISA kits following the manufacturer's protocol. The absorbance was measured using a BioTek ELISA reader (EPOCH II software) at 450 nm.

Western blot analysis

Lung tissues were homogenized in RIPA lysis buffer supplemented with a protease inhibitor cocktail and phenylmethylsulfonyl fluoride (PMSF) to ensure protein stability. The homogenates were centrifuged, and the supernatants were carefully collected for protein analysis. Protein concentrations were determined via a BCA protein assay kit (Rockford, IL, USA), with bovine serum albumin (BSA) used as the standard.

For SDS-PAGE, 30 µg of total protein from each sample was mixed with Laemmli sample buffer, denatured by boiling, and separated on 10% polyacrylamide gels. Proteins were then transferred to polyvinylidene fluoride (PVDF) membranes. To block nonspecific binding, the membranes were incubated with 5% BSA in TBST (Tris-buffered saline with Tween-20) for 60 min at room temperature.

The membranes were then incubated overnight at 4 ˚C with primary antibodies against β-actin (Cat. No. E-AB-40338), HMGB1 (Cat. No. E-AB-70044), NF-κB (Cat. No. E-AB-32232), HO-1 (Cat. No. AF5393), Nrf2 (Cat. No. BT-AP06174), Keap1 (Cat. No. 31801801), and TLR4 (Cat. No. 94401401). After being washed with PBST, the membranes were incubated with horseradish peroxidase (HRP)-conjugated goat anti-mouse IgG secondary antibody (1:2000; sc-2005) for 90 min at room temperature. The protein bands were visualized via enhanced chemiluminescence (ECL) substrate and imaged with a Bio-Rad GelDoc XR detection system (Model: 10000076955, USA). Densitometric analysis was performed, and relative protein expression levels were calculated as fold changes relative to those in the control group (29).

Histopathological examinations

At the end of the experiment, lung tissues were immediately collected and fixed in 10% formaldehyde solution for 48 hr. After fixation, the tissues were embedded in paraffin blocks, and 4 μm-thick sections were prepared. The tissue sections were stained with hematoxylin and eosin (H&E) and examined under a light microscope (Leica DM1000, Germany) at 40x magnification. The severity of tissue damage was assessed semiquantitatively, with a score scale ranging from 0 (normal), 1--10 (mild), 11--20 (moderate), to 21--30 (severe).

Immunofluorescence examinations

For immunofluorescence analysis, tissue sections mounted on poly-L-lysine-coated slides were deparaffinized and rehydrated through a series of graded alcohols. Endogenous peroxidase activity was blocked by incubating the sections in 3% hydrogen peroxide (H_2O_2) for 10 min. Antigen retrieval was performed by boiling the sections in 1% citrate buffer (pH 6.1) for 30 min, then cooling to room temperature. To prevent nonspecific background staining, the sections were incubated with a protein-blocking solution for 5 min. The primary antibodies used were as follows: 8-OHdG (Cat. No. sc-66036, dilution 1:100, Santa Cruz Biotechnology, USA) and caspase-3 (Cat. No. sc-56053, dilution 1:100, Santa Cruz Biotechnology, USA). After incubation with the primary antibodies, the sections were incubated with the appropriate secondary antibodies: FITC-conjugated goat anti-mouse IgG (Cat. No. ab6785, dilution 1:1000, Abcam, UK) for 45 min in the dark for 8-OHdG and Texas Red-conjugated goat anti-mouse IgG (Cat. No. ab6719, dilution 1:1000, Abcam, UK) for 45 min in the dark for Caspase-3. Finally, the sections were stained with DAPI (Cat. No. D1306, 1:200 dilution, Invitrogen, UK) for 5 min in the dark to label the nuclei, then mounted with a coverslip. The stained sections were examined via a fluorescence microscope (Zeiss AXIO, Germany).

Molecular docking, MM-GBSA analysis, and pharmacophore mapping analysis

In this study, the binding properties of SA to the KEAP1 receptor against lipopolysaccharide-induced septic lung injury were analyzed *in silico* via the licensed version of Schrödinger Maestro 2025/1 (Schrödinger, 2025). The 5FZN PDB-encoded crystal structure of the KEAP1 receptor was chosen as the protein target. With the Protein Preparation Wizard module, missing hydrogen atoms in the receptor structure were completed, water molecules were removed, and the protonation state was adjusted to pH 7.0. The SA ligands were converted to three-dimensional structures using the LigPrep module, and low-energy conformers were generated. A 20x20x20 Å grid box was placed at the agonist site in the receptor, and molecular docking was performed at the standard precision (SP) level with the Glide module. The binding energies of the complexes obtained after docking were calculated via the Prime MM-GBSA method, and potential pharmacophore sites for SA were analyzed.

Statistical analyses

Statistical analyses were performed using GraphPad Prism 8.0.1 for quantitative data and SPSS 13.0 for histopathological evaluations. Immunohistochemical and immunofluorescence analyses were conducted via ZEISS Zen Imaging Software. One-way analysis of variance (ANOVA) followed by Duncan's multiple-range test was used to compare group differences. A *P*-value of <0.05 was considered to indicate statistical significance. The data are expressed as the means±standard errors of the means (SEMs).

Results

Effects of SA and LPS on the live and lung weights of the rats

The initial and final body weights, as well as the lung weights, of the rats are presented in Table 1. No significant differences in initial body weight were observed among the experimental groups ($P>0.05$). At the end of the experiment, rats in the LPS, SA40+LPS, and SA80+LPS groups had significantly lower final body weights compared with the control ($P<0.01$). Lung weights were significantly higher in the LPS group than in all other groups ($P<0.001$).

Effects of SA on oxidant and anti-oxidant parameters in LPS-induced septic lung injury

As shown in Figure 1, MDA levels in lung tissues were

Table 1. Initial and final body weights and lung weights of rats (mean±SEM; n=12)

Parameters	Groups				
	Control	SA80	LPS	SA40+LPS	SA80+LPS
Initial body weights (g)	273.25±5.89 [a]	269.00±3.63 [a]	275.12±7.43 [a]	272.50±1.89 [a]	269.37±5.42 [a]
Final body weights (g)	314.38±7.48 [a]	304.00±3.60 [b]	289.13±7.43 [c]	291.50±2.11 [c]	289.38±5.42 [c]
Lung weights (g)	2.40 ±.0.15 [b]	2.03±0.17 [b]	3.14±0.19 [a]	2.57±0.16 [b]	2.03±0.17 [b]

Different letters indicate significant differences ($P<0.05$)
SA: Syringic acid; LPS: Lipopolysaccharide

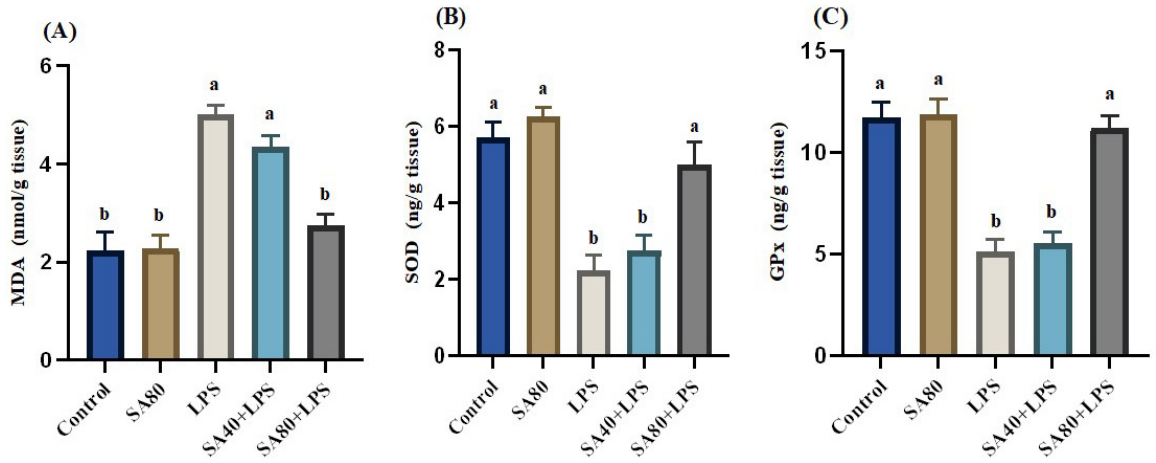

Figure 1. Lung tissue levels of MDA (A), SOD (B), and GPx (C) in control rats, LPS-exposed rats, and LPS-exposed rats treated with SA. All measurements were performed in lung tissue homogenates. Data are presented as mean±SEM (n=12)
Different letters indicate statistically significant differences between groups (P<0.001)
MDA: Malondialdehyde; SOD: Superoxide dismutase; GPx: Glutathione peroxidase; SA: Syringic acid; LPS: Lipopolysaccharide

significantly elevated in the LPS and SA40+LPS groups compared with those in the control group (P<0.001). The administration of SA reduced MDA levels in a dose-dependent manner. Notably, the MDA levels in the SA80+LPS and SA80 groups were comparable to those in the control group. The SA80+LPS levels were comparable to those of the control (P>0.05). SOD and GPx activities were significantly decreased in LPS (P<0.001), but were restored in the SA80+LPS and SA80 groups (P>0.05 vs control).

Effects of SA on LPS-induced lung inflammation

As shown in Figure 2, the IL-1β and IL-6 levels in the lung tissue were significantly elevated in the LPS and SA40+LPS groups compared with those in the other groups (P<0.01), while SA80+LPS levels were lower than LPS (P<0.05) but slightly above control (P>0.05). TNF-α was highest in LPS (P<0.001), intermediate in SA40+LPS (P<0.05 vs LPS), and lowest in SA80+LPS and SA80 groups (P>0.05 vs control).

Effect of SA on the HMGB1/TLR4/NF-κB pathway in the lungs of LPS-treated rats

As shown in Figure 3, the protein expression levels of HMGB1, TLR4, and NF-κB were significantly greater in the LPS group than in the control group (P<0.01). SA administration, mainly at the higher dose (SA80+LPS), markedly reduced the expression of these proinflammatory signaling proteins (P<0.001), approaching control levels (P>0.05). These findings suggest that SA attenuates LPS-induced lung inflammation by modulating the HMGB1/TLR4/NF-κB signaling pathway in a dose-dependent manner.

Effect of SA on the Keap1/Nrf2/HO-1 pathway in the lungs of LPS-treated rats

As shown in Figure 4, Keap1 protein expression was significantly elevated in the LPS group compared with the other groups (P<0.001), whereas the lowest expression was observed in the SA80+LPS group (P<0.001). In contrast, Nrf2 and HO-1 protein levels were significantly reduced in the LPS group (P<0.001) but markedly increased in the SA80+LPS group (P<0.001 vs LPS). Compared with the LPS group, the SA group, chiefly the 80 mg/kg SA group, presented significantly up-regulated Nrf2 and HO-1 expression, indicating activation of anti-oxidant defense mechanisms in response to SA treatment.

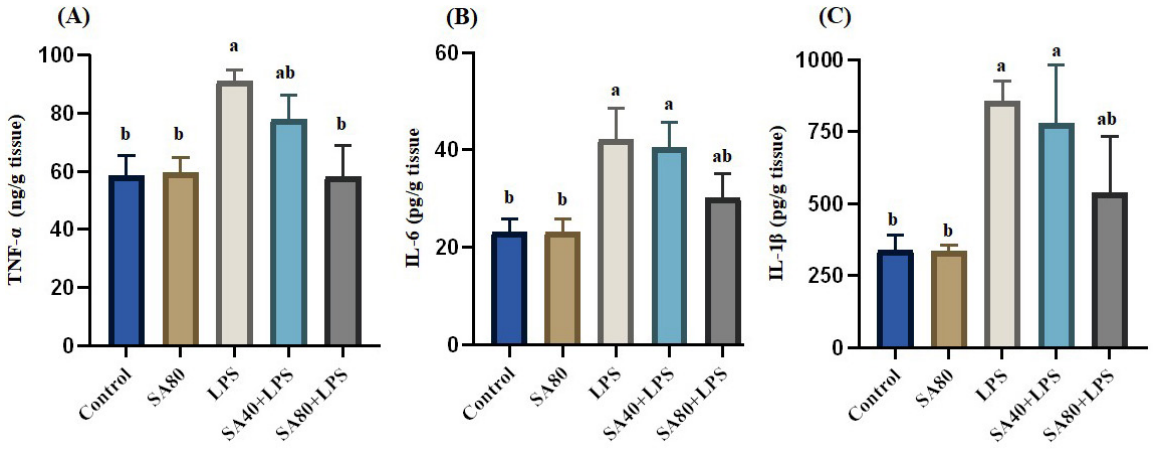

Figure 2. Lung tissue levels of TNF-α (A), IL-6 (B), and IL-1β (C) in control rats, LPS-exposed rats, and LPS-exposed rats treated with SA. All measurements were performed in lung tissue homogenates. Data are presented as mean±SEM (n=12)
Different letters indicate statistically significant differences between groups (P<0.01)
SA: Syringic acid; LPS: Lipopolysaccharide

Histopathological findings

The histopathological findings are presented in Figure 5 and Table 2. Examination of lung tissues from the control and SA80 groups revealed a standard histological structure. In contrast, lung tissues from the LPS group presented severe degeneration, desquamation, and necrosis in the bronchial and bronchiolar epithelium (P<0.001 vs control). Additionally, there was infiltration of mononuclear cells, thickening of the interstitial spaces due to inflammation, and marked hyperemia in the blood vessels. The lung tissues

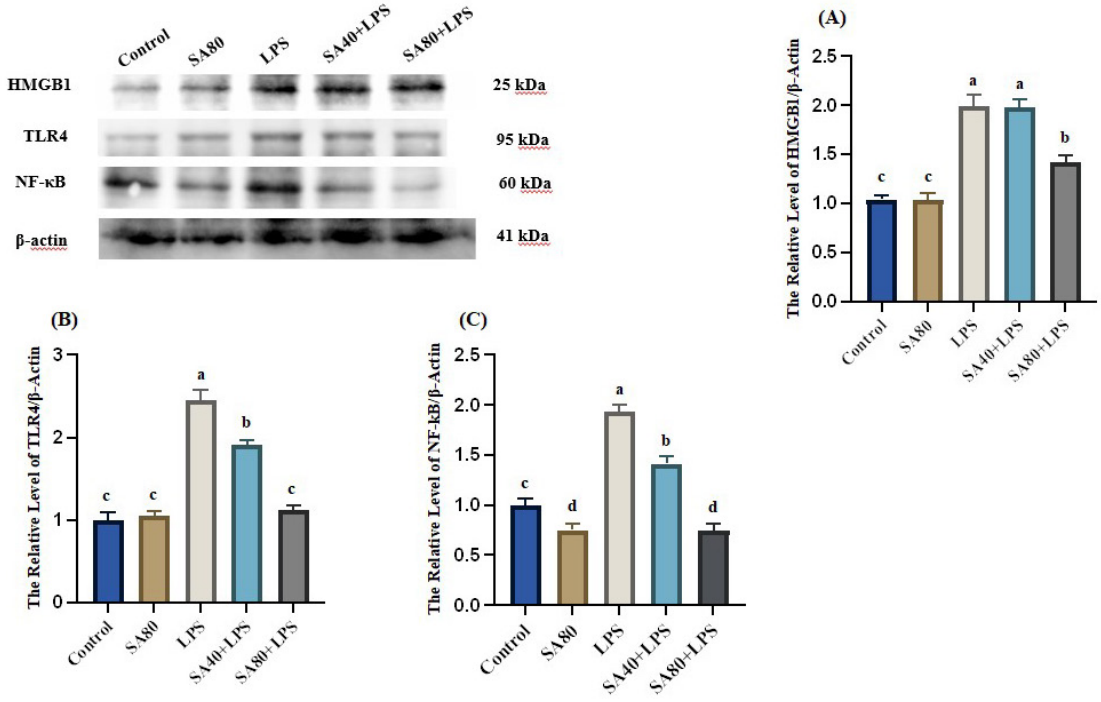

Figure 3. Western blot analysis of HMGB1 (A), TLR4 (B), and NF-κB (C) protein expression in lung tissues of control rats, LPS-exposed rats, and LPS-exposed rats treated with SA. Protein levels were normalized to β-actin and are expressed as relative protein expression (mean±SEM, n=12)
Different letters indicate statistically significant differences between groups (P<0.001)
SA: Syringic acid; LPS: Lipopolysaccharide

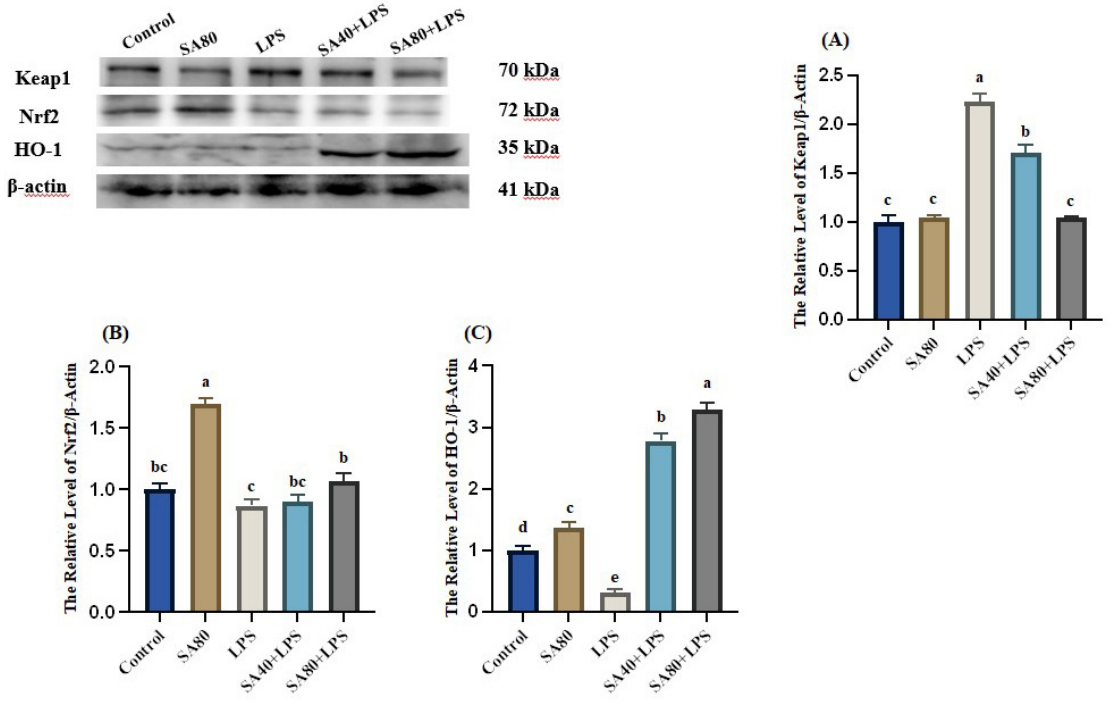

Figure 4. Western blot analysis of Keap1 (A), Nrf2 (B), and HO-1 (C) protein expression in lung tissues of control rats, LPS-exposed rats, and LPS-exposed rats treated with SA. Protein levels were normalized to β-actin and are expressed as relative protein expression (mean±SEM, n=12)
Different letters indicate statistically significant differences between groups (P<0.001)
SA: Syringic acid; LPS: Lipopolysaccharide

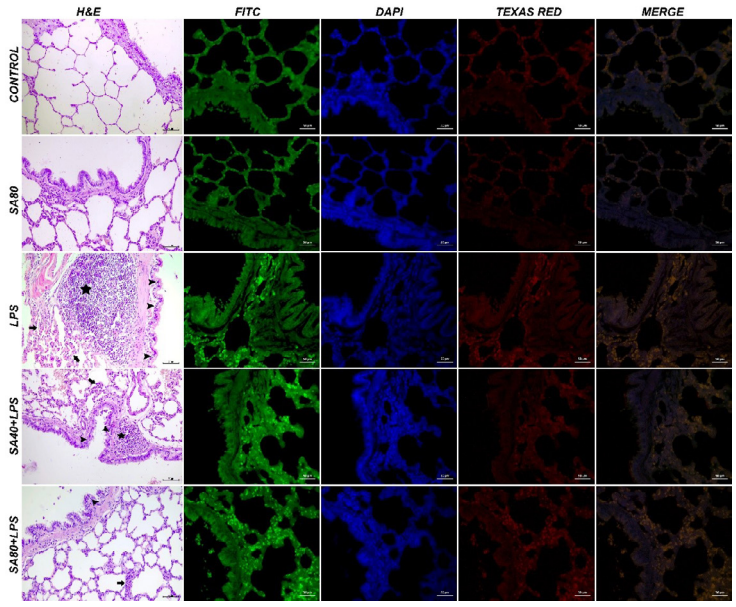

Figure 5. Representative rat lung histological sections stained with hematoxylin and eosin (H&E; scale bar = 70 µm) showing inflammation (asterisk), epithelial degeneration (arrowheads), and interstitial thickening (arrows) in control rats, LPS-exposed rats, and LPS-exposed rats treated with SA, together with immunofluorescence images of 8-OHdG (FITC, green) and caspase-3 (Texas Red, red). Nuclei were counterstained with DAPI (blue); scale bar=50 µm
SA: Syringic acid; LPS: Lipopolysaccharide

from the SA40+LPS group exhibited moderate degeneration of the bronchial and bronchiolar epithelium, thickening of the interstitial spaces due to inflammation, moderate hyperemia, and hemorrhaging of the vessels (P<0.05 vs LPS). In the SA80+LPS group, mild degeneration of the bronchial and bronchiolar epithelium, mild thickening of the interalveolar septa, and mild hyperemia of the blood vessels were observed (P>0.05).

Immunofluorescence findings

Immunofluorescence analysis of 8-OHdG and Caspase-3 expression in lung tissues is presented in Figure 5 and Table 3. No detectable expression of 8-OHdG or Caspase-3 was detected in the control or SA80 groups, indicating minimal oxidative DNA damage and apoptotic activity. In contrast, the LPS group showed intense immunofluorescent labeling of both markers (P<0.001), particularly those localized to the bronchial and bronchiolar epithelium, reflecting significant oxidative stress and apoptosis. The SA40+LPS group presented moderate expression levels (P<0.05 vs LPS), whereas the SA80+LPS group presented only mild immunoreactivity for both markers (P>0.05 vs control). Compared with the LPS group, reductions in 8-OHdG and caspase-3 expression in the SA-treated groups were statistically significant (P<0.05), indicating that SA exerted a dose-dependent protective effect.

Table 3. Quantification of 8-OHdG and Caspase-3 expression in rat lung tissues (mean±SEM, n=12)

Experimental groups	8-OHdG	Caspase-3
Control	23.42±1.87 [d]	19.23±2.2 [d]
SA80	25.57±2.12 [d]	20.03±1.03 [d]
LPS	86.54±3.74 [a]	71.57±4.58 [a]
SA40+LPS	68.12±4.51 [b]	51.39±3.81 [b]
SA80+LPS	42.29±2.39 [c]	38.00±2.98 [c]

Different letters indicate significant differences (P<0.05)
SA: Syringic acid; LPS: Lipopolysaccharide

In silico analysis of SA binding to the KEAP1 Kelch domain

To explore the molecular mechanism underlying SA's anti-oxidant effects, *in silico* docking was performed with the KEAP1 Kelch domain, a critical regulator of Nrf2. SA

Table 4. Histopathological scoring of rat lung tissues

Experimental groups	Degeneration of bronchial-bronchiole epithelium	Thickening of the interalveolar septum	Hyperemia in vessels
Control group	-	-	-
SA80 group	-	-	-
LPS group	+++	+++	+++
SA40+LPS group	++	++	+++
SA80+LPS group	+	+	++

Scores: (-) none, (+) mild, (++) moderate, (+++) severe
SA: Syringic acid; LPS: Lipopolysaccharide

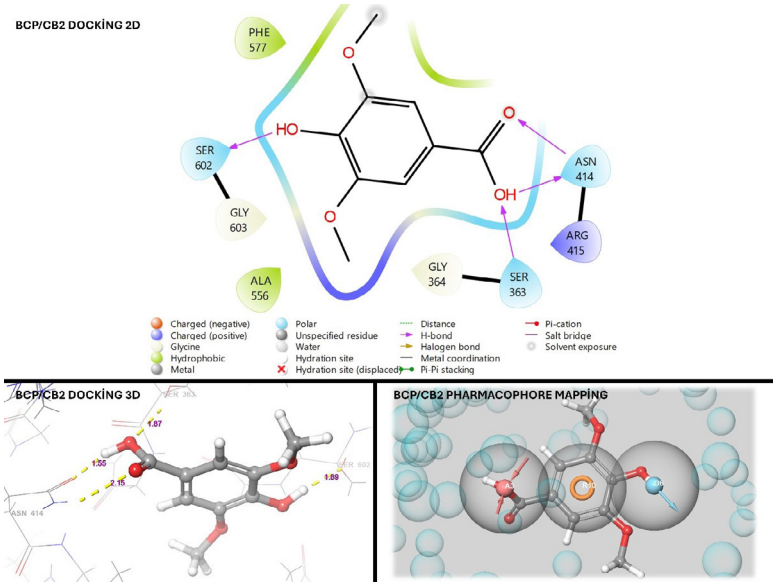

Figure 6. Molecular docking of syringic acid (SA) with the KEAP1 Kelch domain: (A) 2D interaction map showing hydrogen bonds and hydrophobic contacts, (B) 3D docking pose, (C) pharmacophore mapping highlighting key interactions

showed a favorable binding score (-6.72) and formed multiple hydrogen bonds with key residues (SER602, SER363, ASN414), inDicating stable interactions within the KEAP1 pocket (Figure 6, Tables 4-7). MM-GBSA calculations further supported a thermodynamically favorable binding (ΔG_bind=-22.99 kcal/mol). Pharmacophore mapping identified two hydrogen bond acceptors (A3, D6) and a hydrophobic aromatic interaction (R10) as key features stabilizing the SA-KEAP1 complex.

These findings suggest that SA can effectively occupy the KEAP1 inhibitory site, potentially preventing Nrf2 ubiquitination and promoting its nuclear translocation. This molecular interaction aligns with our *in vivo* observations of enhanced Nrf2/HO-1 signaling following SA treatment, providing a mechanistic basis for its dual anti-oxidant and anti-inflammatory effects in LPS-induced lung injury.

Table 4. Docking scores and Glide energy for syringic acid (SA) binding to the KEAP1 Kelch domain

Binding Scores	SA/KEAP1
Docking Scores	-6.71547
Glide Energy	30.8917

Table 5. Hydrogen bond interactions between syringic acid (SA) and KEAP1 residues, showing atom pairs and distances (Å)

Docking complex	Aminoacid	Atom1 (receptor)	Atom2 (ligand)	Distance (angstrom = Å)
	SER602	O:2155	H:4375	1.89
	SER363	H:2520	O:4362	1.87
SA/KEAP1	ASN414	H:2845	O:4363	2.15
	ASN414	O:680	H:4382	1.55

Table 6. Molecular Mechanics–Generalized Born Surface Area (MM-GBSA) binding energy components for the syringic acid (SA)–Kelch-like ECH-associated protein 1 (KEAP1) complex (kcal/mol)

MM-GBSA Results	SA/KEAP1
r_psp_MMGBSA_dG_Bind	-22.99
r_psp_MMGBSA_dG_Bind_Coulomb	-25.53
r_psp_MMGBSA_dG_Bind_Covalent	17.30
r_psp_MMGBSA_dG_Bind_Hbond	-2.37
r_psp_MMGBSA_dG_Bind_Lipo	-8.47
r_psp_MMGBSA_dG_Bind_Packing	-0.61
r_psp_MMGBSA_dG_Bind_SelfCont	0.00
r_psp_MMGBSA_dG_Bind_Solv_GB	18.52
r_psp_MMGBSA_dG_Bind_Solv_SA	
r_psp_MMGBSA_dG_Bind_vdW	-21.82

Table 7. Pharmacophore features of syringic acid (SA) interactions with KEAP1, including hydrogen bond acceptors and hydrophobic aromatic ring interactions

Rank	Feature Label	Score	X	Y	Z	Type	Num	From Chemscore	Source
1	A3	-1.60	14.66	70.2127	32.7909	A	2	0	HBond
2	D6	-1.33	12.1336	64.0978	32.1747	D	5	0	HBond
3	R10	-0.72	13.642	66.9653	31.7454	R	9	0	RingChemscoreHphobe

Discussion

ALI, particularly when triggered by endotoxins such as LPS, is a significant cause of morbidity and mortality due to its multifaceted pathogenesis involving oxidative stress, inflammation, and apoptosis. LPS, a structural component of the outer membranes of Gram-negative bacteria, can enter the bloodstream and elicit a systemic inflammatory response that leads to septic shock and multiple organ dysfunction (30). In experimental research, IP LPS injection is widely used to model ALI in rodents because of its ability to replicate many hallmarks of human sepsis-induced lung damage reliably.

In our study, rats exposed to LPS presented significantly increased lung weights, indicating pulmonary edema, a hallmark of vascular leakage and inflammatory infiltration (31). This increase was notably attenuated in SA-treated groups, suggesting that SA mitigated LPS-induced lung injury at the gross anatomical level.

The observed protective effects of SA appear to stem from its ability to counteract oxidative stress, a central feature of LPS-induced ALI. The overproduction of ROS leads to lipid peroxidation and disruption of cellular homeostasis, as evidenced by elevated levels of MDA, a key biomarker of oxidative membrane damage (32). Similar increases in MDA have been reported in models of LPS-induced lung injury, with compounds such as pterostilbene, SA, and trillin showing efficacy in reducing these levels (32-34). Meng *et al.* (2018) reported a reduction in MDA with dexmedetomidine treatment in ALI (35). Consistent with these findings, our data demonstrated a significant LPS-induced increase in MDA, which was reversed by SA in a dose-dependent manner, underscoring its anti-oxidant capacity. These findings are consistent with studies on aminoguanidine, an iNOS inhibitor, which reduced oxidative stress markers, including MDA, and enhanced anti-oxidant defenses in LPS-challenged lungs (36).

In addition to elevated lipid peroxidation, LPS exposure also suppressed endogenous anti-oxidant defenses, including SO and GPx. These enzymes are essential for neutralizing ROS and protecting tissue integrity. The restoration of SOD and GPx levels by SA aligns with previous reports demonstrating the protective anti-oxidant roles of natural compounds in ALI (33-35). These findings reinforce SA's role as a potent free radical scavenger and redox balance regulator.

A major mechanistic contributor to SA's anti-oxidant action appears to be its regulation of the Nrf2/Keap1/HO-1 signaling axis. Under oxidative conditions, Nrf2 dissociates from its repressor Keap1 and translocates to the nucleus, where it binds to anti-oxidant response elements (AREs) to promote the expression of detoxifying enzymes such as HO-1. Previous studies have shown that LPS disrupts this pathway, increasing Keap1 levels and reducing Nrf2 and HO-1 expression (37, 38). In our study, SA treatment effectively restored this pathway, reducing Keap1 and enhancing Nrf2 activation and HO-1 expression. These results are further supported by those of Somade *et al.* (2023), who reported similar regulatory effects of SA in testicular tissue (39). This restoration of the Nrf2 axis likely underlies SA's protective anti-oxidant effect in lung tissue.

In addition to oxidative stress, inflammation is a key pathological driver of LPS-induced lung injury. Central to this inflammatory cascade is the activation of TLR4 by LPS, which in turn activates NF-κB signaling and induces the release of HMGB1, TNF-α, IL-1β, and IL-6—cytokines that amplify tissue damage and immune cell infiltration (40-45). In agreement with studies by Liu *et al.* (2019), Huang *et al.* (2020), and Alsharif *et al.* (2021), we observed marked increases in these inflammatory mediators following LPS exposure (17, 46, 47). Significantly, SA treatment substantially attenuated this cytokine surge, confirming its anti-inflammatory efficacy. Similarly, a previous study by Boskabady *et al.* (2018) reported that captopril modulated pro- and anti-inflammatory cytokines and restored Th1/Th2 balance in LPS-induced lung injury, paralleling the anti-inflammatory effects observed with SA in our study (48). Moreover, thymoquinone reduced pro-inflammatory cytokines, restored anti-inflammatory IL-4, and improved lung histopathology in LPS-exposed rats, further supporting the relevance of natural compounds with dual anti-oxidant and anti-inflammatory actions in mitigating ALI (49). Additionally, aerobic exercise has been shown to attenuate LPS-induced lung injury in rodent models by reducing oxidative stress, decreasing pro-inflammatory cytokines, increasing anti-inflammatory mediators such as IL-10, and improving lung histopathology, highlighting that multi-target strategies beyond pharmacological interventions can confer protection in ALI (50). Furthermore, our current study demonstrated that SA inhibits the HMGB1/TLR4/NF-κB axis, consistent with the findings of Demir *et al.* (2023) and He *et al.* (2025), who reported that modulation of this pathway is critical for reducing inflammation in ALI models (51, 52). To our knowledge, this study is the first to report that SA alleviates lung inflammation by suppressing this pathway in the context of LPS-induced injury.

In addition to preventing inflammation and oxidative stress, SA also confers protection against DNA damage and apoptosis, two additional consequences of ROS accumulation. Elevated levels of 8-OHdG, a sensitive marker of oxidative DNA damage, and caspase-3, a central executioner of apoptosis, were observed in the LPS-treated rats. These findings are consistent with earlier studies by Yan *et al.* (2017), Fu *et al.* (2017), and Okkay *et al.* (2022), which reported similar biomarker elevations following LPS

administration (53-55). SA treatment significantly reduced both 8-OHdG and caspase-3 expression levels, suggesting that it not only mitigates oxidative insult but also prevents downstream cellular apoptosis.

Collectively, our findings illustrate that SA exerts multifaceted protective effects against LPS-induced ALI by modulating key molecular pathways. Its phenolic structure enables direct ROS scavenging, while its biological activity promotes Nrf2-mediated transcription of anti-oxidant defenses and suppresses HMGB1/TLR4/NF-κB-mediated inflammation. This dual action not only stabilizes cellular membranes but also reduces inflammatory cytokine production, DNA damage, and apoptosis. The observed preservation of lung architecture in the SA-treated groups, coupled with the significant biochemical and molecular changes, strongly supports its therapeutic potential.

Consistent with the *in vivo* data, our *in silico* molecular docking analysis further supported the mechanistic role of SA in modulating oxidative stress pathways. Computational modeling revealed a strong binding affinity of SA to the Kelch domain of KEAP1, a critical negative regulator of Nrf2. This interaction was stabilized through hydrogen bonds and hydrophobic contacts, indicating that SA may prevent the proteasomal degradation of Nrf2 by sterically hindering KEAP1–Nrf2 binding. This mode of action is analogous to that of synthetic inhibitors and cyclic peptides shown to reduce oxidative damage in experimental ALI models (56).

The *in silico* findings therefore reinforce the hypothesis that SA's anti-oxidant efficacy arises not only from direct ROS scavenging but also from upstream stabilization of Nrf2, offering a plausible molecular explanation for the biochemical and histological improvements observed in our animal model.

In summary, this study provides the first comprehensive evidence that SA effectively attenuates LPS-induced ALI through dual modulation of oxidative stress and inflammation. SA enhances anti-oxidant defenses by activating the Keap1/Nrf2/HO-1 pathway and suppresses inflammatory signaling by inhibiting the HMGB1/TLR4/NF-κB axis. *In silico* docking further revealed a mechanistic interaction between SA and the KEAP1 Kelch domain, suggesting a direct role in stabilizing Nrf2 activity. These findings underscore the therapeutic potential of SA as a multitarget agent for managing sepsis-associated lung injury and other inflammation-related pulmonary conditions.

Limitations

This study has several limitations that warrant consideration. First, although SA demonstrated protective effects against LPS-induced ALI in rats, the precise pharmacokinetic profile of SA, including its bioavailability and *in vivo* metabolic fate, was not evaluated. Second, the study relied on a single acute time point (12 hr post-LPS challenge), which may not fully capture the dynamic progression or resolution of lung injury. Lastly, extrapolation of these findings to human physiology should be made cautiously, as species-specific differences may affect the translational relevance of the results. Future studies integrating chronic models, broader time-course analyses, and genetic or pharmacologic intervention strategies are necessary to further substantiate the therapeutic potential of SA.

Conclusion

This study provides strong evidence that SA protects against LPS-induced ALI through dual regulation of oxidative stress and inflammation. SA enhanced anti-oxidant defenses by activating the Keap1/Nrf2/HO-1 pathway and suppressed pro-inflammatory signaling via inhibition of the HMGB1/TLR4/NF-κB axis. In addition, SA reduced lipid peroxidation, DNA damage, and apoptosis, thereby preserving lung tissue integrity. Molecular docking further supported these findings by revealing a direct interaction between SA and the KEAP1 Kelch domain, suggesting stabilization of Nrf2 activity. Collectively, these results highlight the therapeutic potential of SA as a multitarget agent for sepsis-associated and inflammation-related pulmonary disorders.

Acknowledgment

The results described in this paper are part of Burak Batuhan Lacin's thesis.

Funding

This research was supported by the Scientific Research Projects Coordination Unit of Atatürk University under Project No: TDK-2022/11637. The authors extend their sincere gratitude to Atatürk University, Erzurum, Turkey, for its continuous support and valuable contributions to this study.

Data Availability Statement

The data supporting the findings of this study are available from the corresponding authors upon request.

Authors' Contributions

BB L conducted the experimental work, curated the data, and contributed to the preparation of the original draft. E S supervised the development of the methodology and contributed to data analysis and interpretation. S Y performed histopathological and immunofluorescence analyses and evaluated the results. F A assisted with experimental design, sample preparation, and laboratory analysis. M W contributed to the conceptualization, critical review, and editing of the manuscript, as well as the funding acquisition strategy. B C performed *in silico* analyses and evaluated the results. A C handled conceptualization, project administration, overall supervision, and final manuscript editing.

Conflicts of Interest

The authors declare that they have no conflicts of interest.

Declaration

The authors acknowledge the use of ChatGPT (OpenAI, San Francisco, CA, USA) to improve the language clarity and style of the manuscript. The authors are fully responsible for the content and interpretations presented.

References

1. Delano MJ, Ward PA. The immune system's role in sepsis progression, resolution, and long-term outcome. Immunol Rev 2016; 274: 330-353.
2. Confalonieri M, Salton F, Fabiano F. Acute respiratory distress syndrome. Eur Respir Rev 2017; 26: 160116-160123.
3. Chopra M, Reuben JS, Sharma AC. Acute lung injury: Apoptosis

and signaling mechanisms. Exp Biol Med 2009; 234: 361-371.
4. Tang J, Xu L, Zeng Y, Gong F. Effect of gut microbiota on LPS-induced acute lung injury by regulating the TLR4/NF-kB signaling pathway. Int Immunopharmacol 2021; 91: 107272.
5. Sul O-J, Ra SW. Quercetin prevents LPS-induced oxidative stress and inflammation by modulating NOX2/ROS/NF-kB in lung epithelial cells. Molecules 2021; 26: 6949-6960.
6. Liang P, Zhou S, Yuan Z, Zhang L, Jiang Z, Yu Q. Obeticholic acid improved triptolide/lipopolysaccharide- induced hepatotoxicity by inhibiting caspase- 11- GSDMD pyroptosis pathway. J Appl Toxicol 2023; 43: 599-614.
7. Shah D, Das P, Acharya S, Agarwal B, Christensen DJ, Robertson SM, *et al.* Small immunomodulatory molecules as potential therapeutics in experimental murine models of acute lung injury (ALI)/acute respiratory distress syndrome (ARDS). Int J Mol Sci 2021; 22: 2573-2591.
8. Fan L, Fan Y, Liu L, Tao W, Shan X, Dong Y, *et al.* Chelerythrine attenuates the inflammation of lipopolysaccharide-induced acute lung inflammation through NF-κB signaling pathway mediated by Nrf2. Front Pharmacol 2018; 9: 1047-1057.
9. Mu X, Hur S. Immunogenicity of *in vitro*-transcribed RNA. Acc Chem Res 2021; 54: 4012-4023.
10. Park WS, Lee J, Na G, Park S, Seo S-K, Choi JS, *et al.* Benzyl isothiocyanate attenuates inflammasome activation in Pseudomonas aeruginosa LPS-stimulated THP-1 cells and exerts regulation through the MAPKs/NF-κB pathway. Int J Mol Sci 2022; 23: 1228.
11. Yue L, Qidian L, Jiawei W, Rou X, Miao H. Acute iron oxide nanoparticles exposure induced murine eosinophilic airway inflammation via TLR2 and TLR4 signaling. Environ Toxicol 2022; 37: 925-935.
12. Xue J, Suarez JS, Minaai M, Li S, Gaudino G, Pass HI, *et al.* HMGB1 as a therapeutic target in disease. J Cell Physiol 2021; 236: 3406-3419.
13. Ding X, Li S, Zhu L. Potential effects of HMGB1 on viral replication and virus infection-induced inflammatory responses: A promising therapeutic target for virus infection-induced inflammatory diseases. Cytokine Growth Factor Rev 2021; 62: 54-61.
14. Ge Y, Huang M, Yao Y-m. The effect and regulatory mechanism of high mobility group box-1 protein on immune cells in inflammatory diseases. Cells 2021; 10: 1044-1070.
15. Caldeira C, Cunha C, Vaz AR, Falcão AS, Barateiro A, Seixas E, *et al.* Key aging-associated alterations in primary microglia response to beta-amyloid stimulation. Front Aging Neurosci 2017; 9: 277-300.
16. Chang H-Y, Chen Y-C, Lin J-G, Lin I-H, Huang H-F, Yeh C-C, *et al.* Asatone prevents acute lung injury by reducing expressions of NF-κ B, MAPK and inflammatory cytokines. Am J Chin Med 2018; 46: 651-671.
17. Huang C-Y, Deng J-S, Huang W-C, Jiang W-P, Huang G-J. Attenuation of lipopolysaccharide-induced acute lung injury by hispolon in mice, through regulating the TLR4/PI3K/Akt/mTOR and Keap1/Nrf2/HO-1 pathways, and suppressing oxidative stress-mediated ER stress-induced apoptosis and autophagy. Nutrients 2020; 12: 1742-1764.
18. Luo L, Huang F, Zhong S, Ding R, Su J, Li X. Astaxanthin attenuates ferroptosis via Keap1-Nrf2/HO-1 signaling pathways in LPS-induced acute lung injury. Life Sci 2022; 311:121091.
19. Jadeja RN, Upadhyay KK, Devkar RV, Khurana S. Naturally occurring Nrf2 activators: Potential in treatment of liver injury. Oxid Med Cell Longev 2016; 2016: 3453926-3453939.
20. Nguyen T, Nioi P, Pickett CB. The Nrf2-antioxidant response element signaling pathway and its activation by oxidative stress. Journal of biological chemistry 2009; 284:13291-13295.
21. Schönthal AH. Endoplasmic reticulum stress: Its role in disease and novel prospects for therapy. Scientifica 2012; 2012: 857516-857542.
22. Shi C, Sun Y, Zheng Z, Zhang X, Song K, Jia Z, *et al.* Antimicrobial activity of syringic acid against Cronobacter sakazakii and its effect on cell membrane. Food Chem 2016; 197: 100-106.
23. Srinivasulu C, Ramgopal M, Ramanjaneyulu G, Anuradha C, Kumar CS. Syringic acid (SA)–a review of its occurrence, biosynthesis, pharmacological and industrial importance. Biomed Pharmacother 2018; 108: 547-557.
24. Ji J, Yang X, Flavel M, Shields ZP-I, Kitchen B. Antioxidant and anti-diabetic functions of a polyphenol-rich sugarcane extract. J Am Coll Nutr 2019; 38: 670-680.
25. Rashedinia M, Alimohammadi M, Shalfroushan N, Khoshnoud MJ, Mansourian M, Azarpira N, *et al.* Neuroprotective effect of syringic acid by modulation of oxidative stress and mitochondrial mass in diabetic rats. Biomed Res Int 2020; 2020: 8297984-829796.
26. Periyannan V, Veerasamy V. Syringic acid may attenuate the oral mucosal carcinogenesis via improving cell surface glycoconjugation and modifying cytokeratin expression. Toxicol Rep 2018; 5: 1098-1106.
27. Gheena S, Ezhilarasan D, Shree Harini K, Rajeshkumar S. Syringic acid and silymarin concurrent administration inhibits sodium valproate- induced liver injury in rats. Environ Toxicol 2022; 37: 2143-2152.
28. Köse D, Yüksel TN, Halıcı Z, Çadırcı E, Gürbüz MA. The effects of agomelatine treatment on lipopolysaccharide-induced septic lung injuries in rats. Eurasian J Med 2021; 53: 127-131.
29. Bass JJ, Wilkinson DJ, Rankin D, Phillips BE, Szewczyk NJ, Smith K, *et al.* An overview of technical considerations for Western blotting applications to physiological research. Scand J Med Sci Sports 2017; 27: 4-25.
30. Niu X, Mu Q, Li W, Huang H, Yao H, Li H. Protective effects of chelerythrine against lipopolysaccharide-induced endotoxic shock in mice. Inflammation 2014; 37: 1968-1975.
31. Zhang Y, Du Z, Zhou Q, Wang Y, Li J. Remifentanil attenuates lipopolysaccharide-induced acute lung injury by downregulating the NF-κB signaling pathway. Inflammation 2014; 37: 1654-1660.
32. Jiang W, Luo F, Lu Q, Liu J, Li P, Wang X, *et al.* The protective effect of Trillin LPS-induced acute lung injury by the regulations of inflammation and oxidative state. Chem Biol Interact 2016; 243: 127-134.
33. Zhang Y, Han Z, Jiang A, Wu D, Li S, Liu Z, *et al.* Protective effects of pterostilbene on lipopolysaccharide-induced acute lung injury in mice by inhibiting NF-κB and activating Nrf2/HO-1 signaling pathways. Front Pharmacol 2021; 11: 591836-591848.
34. Li Y, Zhang L, Wang X, Wu W, Qin R. Effect of Syringic acid on antioxidant biomarkers and associated inflammatory markers in mice model of asthma. Drug Dev Res 2019; 80: 253-261.
35. Meng L, Li L, Lu S, Li K, Su Z, Wang Y, *et al.* The protective effect of dexmedetomidine on LPS-induced acute lung injury through the HMGB1-mediated TLR4/NF-κB and PI3K/Akt/mTOR pathways. Mol Immunol 2018; 94: 7-17.
36. Saadat S, Beheshti F, Askari VR, Hosseini M, Mohamadian Roshan N, Boskabady MH. Aminoguanidine affects systemic and lung inflammation induced by lipopolysaccharide in rats. Respir Res 2019; 20: 96-109.
37. Hong H, Lou S, Zheng F, Gao H, Wang N, Tian S, *et al.* Hydnocarpin D attenuates lipopolysaccharide-induced acute lung injury via MAPK/NF-κB and Keap1/Nrf2/HO-1 pathway. Phytomedicine 2022; 101: 154143.
38. Zhao L, Zhang Z, Li P, Gao Y, Shi Y. Bakuchiol regulates TLR4/MyD88/NF-κB and Keap1/Nrf2/HO-1 pathways to protect against LPS-induced acute lung injury *in vitro* and *in vivo*. Naunyn Schmiedebergs Arch Pharmacol 2024; 397: 3301-3312.
39. Somade OT, Ajiboye BO, Osukoya OA, Jarikre TA, Oyinloye BE. Syringic acid ameliorates testicular oxidative stress via the conservation of endogenous antioxidant markers and inhibition of the activated Nrf2-Keap1-NQO1-HO1 signaling in methyl cellosolve-administered rats. Pharmacol Res Modern Chin Med 2023; 6: 100207.
40. Kojima M, Gimenes-Junior JA, Chan TW, Eliceiri BP, Baird A, Costantini TW, *et al.* Exosomes in postshock mesenteric lymph are key mediators of acute lung injury triggering the macrophage activation via Toll-like receptor 4. Faseb J 2018; 32: 97-110.

41. Fitzgerald KA, Rowe DC, Barnes BJ, Caffrey DR, Visintin A, Latz E, *et al.* LPS-TLR4 signaling to IRF-3/7 and NF-kappaB involves the toll adapters TRAM and TRIF. J Exp Med 2003; 198: 1043-1055.
42. Ben DF, Yu XY, Ji GY, Zheng DY, Lv KY, Ma B, *et al.* TLR4 mediates lung injury and inflammation in intestinal ischemia-reperfusion. J Surg Res 2012; 174: 326-333.
43. Li L, Zhou B, Xu H, Shi H, Gao L, Ge B. Zinc-loaded black phosphorus multifunctional nanodelivery system combined with photothermal therapy have the potential to treat prostate cancer patients infected with COVID-19. Front Endocrinol (Lausanne) 2022; 13: 872411-872425.
44. Yu H, Lin L, Zhang Z, Zhang H, Hu H. Targeting NF-κB pathway for the therapy of diseases: mechanism and clinical study. Signal Transduct Target Ther 2020; 5: 209-232.
45. Zuo W, Tian F, Ke J, Jiang C, Yang Y, He C. Mechanisms and research progress of traditional chinese medicine regulating NF-κB in the treatment of acute lung injury/acute respiratory distress syndrome. CMNP 2024; 4: e93-e105.
46. Liu J, Huang X, Hu S, He H, Meng Z. Dexmedetomidine attenuates lipopolysaccharide induced acute lung injury in rats by inhibition of caveolin-1 downstream signaling. Biomed Pharmacother 2019; 118: 109314-109321.
47. Alsharif KF, Almalki AA, Alsanie WF, Alzahrani KJ, Kabrah SM, Elshopakey GE, *et al.* Protocatechuic acid attenuates lipopolysaccharide-induced septic lung injury in mice: The possible role through suppressing oxidative stress, inflammation and apoptosis. J Food Biochem 2021; 45: e13915.
48. Boskabadi J, Askari VR, Hosseini M, Boskabady MH. Immunomodulatory properties of captopril, an ACE inhibitor, on LPS-induced lung inflammation and fibrosis as well as oxidative stress. Inflammopharmacology 2018; 27: 639-647.
49. Boskabady M, Khazdair MR, Bargi R, Saadat S, Memarzia A, Mohammadian Roshan N, *et al.* Thymoquinone ameliorates lung inflammation and pathological changes observed in lipopolysaccharide-induced lung injury. Evid Based Complement Alternat Med 2021; 2021: 6681729-6681739.
50. Gholamnezhad Z, Safarian B, Esparham A, Mirzaei M, Esmaeilzadeh M, Boskabady MH. The modulatory effects of exercise on lipopolysaccharide-induced lung inflammation and injury: A systemic review. Life Sci 2022; 293: 120306.
51. He X, Chen GF, Tao WT, Huang XJ, Lin Y, Sun J, *et al.* Tetramethylpyrazine mitigates lipopolysaccharide-induced acute lung injury by inhibiting the HMGB1/TLR4/NF-κB signaling pathway in mice. J Thorac Dis 2025; 17: 1605-1616.
52. Demir EA, Demir S, Kazaz IO, Kucuk H, Alemdar NT, Gecici OF, *et al.* Syringic acid ameliorates ischemia/reperfusion-induced testicular injury in rats via suppressing of HMGB1/NF-κB axis and endoplasmic reticulum stress. Eur J Trauma Emerg Surg 2023; 49: 1595-1602.
53. Yan X, Cheng X, Zhou L, He X, Zheng W, Chen H. Dexmedetomidine alleviates lipopolysaccharide-induced lung injury in Wistar rats. Oncotarget 2017; 8: 44410-44417.
54. Okkay IF, Okkay U, Gundogdu OL, Bayram C, Mendil AS, Ertugrul MS, *et al.* Syringic acid protects against thioacetamide-induced hepatic encephalopathy: Behavioral, biochemical, and molecular evidence. Neurosci Lett 2022; 769: 136385.
55. Fu C, Dai X, Yang Y, Lin M, Cai Y, Cai S. Dexmedetomidine attenuates lipopolysaccharide-induced acute lung injury by inhibiting oxidative stress, mitochondrial dysfunction and apoptosis in rats. Mol Med Rep 2017; 15: 131-138.
56. Zou J, Yan J, Lu Y, Yu Z, Zhang K, Han Q, *et al.* Cyclic peptide Keap1-Nrf2 protein-protein interaction inhibitors: Design, synthesis, and *in vivo* treatment of acute lung injury. J Med Chem 2024; 67: 4889-4903.